Archives of Biochemistry and Biophysics
Vol. 383, No. 2, November 15, pp. 157–170, 2000
doi:10.1006/abbi.2000.1993, available online at http://www.idealibrary.com on IDEAL®

Differences in Zero-Force and Force-Driven Kinetics of Ligand Dissociation from β-Galactoside-Specific Proteins (Plant and Animal Lectins, Immunoglobulin G) Monitored by Plasmon Resonance and Dynamic Single Molecule Force Microscopy

Wolfgang Dettmann,* Michel Grandbois,† Sabine André,‡ Martin Benoit,* Angelika K. Wehle,* Herbert Kaltner,‡ Hans-Joachim Gabius,‡ and Hermann E. Gaub*,[1]

*Lehrstuhl für Angewandte Physik, Sektion Physik, Ludwig-Maximilians-Universität München, Amalienstrasse 54, 80799 München, Germany; †Department of Physics and Astronomy, University of Missouri-Columbia, 318 Physics Building, Columbia, Missouri 65211; and ‡Institut für Physiologische Chemie, Tierärztliche Fakultät, Ludwig-Maximilians-Universität München, Veterinärstrasse 13, 80539 München, Germany

Received December 1, 1999, and in revised form June 9, 2000

Protein-carbohydrate interactions are involved in diverse regulatory processes. To help understand the mechanics and kinetics of dissociation of receptor-ligand complexes, we have analyzed the separation of lactose and the *N*-glycan chains of asialofetuin (ASF) from three lectins and an immunoglobulin G fraction by surface plasmon resonance at zero force and by atomic force microscopy with variations of the external force. While the $(AB)_2$ agglutinins from *Ricinus communis* (RCA) and *Viscum album* (VAA) show structural homology, the homodimeric galectin-1 from bovine heart (BHL) has no similarity to the two plant lectins except for sharing this monosaccharide specificity. The β-galactoside-binding immunoglobulin G (IgG) fraction from human serum provides a further model system with distinct binding-site architecture. The k_{off} constants for the two plant agglutinins were independent of the nature of the ligand at 1.1–1.3 × 10^{-3} s^{-1}, whereas the geometry of ligand and binding site presentation affected this parameter for BHL (0.5 × 10^{-3} s^{-1} for lactose and 1 × 10^{-3} s^{-1} for ASF) and IgG (1.3 × 10^{-3} s^{-1} for lactose and 0.55 × 10^{-3} s^{-1} for ASF). When assessing comparatively the rupture forces at a loading rate of 3 nN/s with lactose as ligand, 34 ± 6 pN (BHL), 36 ± 4 pN (IgG), 47 ± 7 pN (VAA), and 58 ± 9 pN (RCA) were measured. For the same loading rate the rupture forces for the receptor-ASF interactions were found to be 37 ± 3 pN (BHL), 43 ± 5 pN (VAA), 45 ± 6 pN (IgG), and 65 ± 9 pN (RCA). The variation of the pulling velocity revealed in all cases a linear dependence between the rupture force and the natural logarithm of the loading rate. Performing probability density and Monte Carlo calculations, the potential barrier widths, which determine the inverse dynamic dependence with the rate of force elevation, increased from 4 Å (RCA) and 7 Å (VAA and IgG) to 10 Å (BHL) for the receptor-lactose interactions. Presenting ASF as ligand potential widths of 4 Å for RCA and IgG and 6 Å for VAA and BHL were obtained. Since the dissociation kinetics at zero force apparently cannot predict the behavior in force-driven experiments, these results reveal new insights into biological functions. The dissociation kinetics under force helps to explain the difference in the toxic potency of VAA and RCA and points to a function of the galectin in *cis*-crosslinking and in transient *trans*-bridging. © 2000 Academic Press

Key Words: **AFM; agglutinin; force spectroscopy; galectin; glycoprotein; lectin; plasmon resonance.**

Rupture forces of biological receptor-ligand pairs are routinely investigated using atomic force microscopy (AFM)[2] and related techniques. The feasibility of as-

[1] To whom correspondence should be addressed. E-mail: gaub@physik.uni-muenchen.de.

[2] Abbreviations used: AFM, atomic force microscopy; ASF, asialofetuin; BHL, bovine heart lectin, galectin-1; CRD, carbohydrate

0003-9861/00 $35.00
Copyright © 2000 by Academic Press
All rights of reproduction in any form reserved.

sessing rupture forces initially was documented for the biotin/avidin (streptavidin) system (1, 2) and for several antibody/antigen pairs (3–6). This experimental approach explores the ability of biomolecular associations to withstand force and complements descriptions of classical equilibrium thermodynamics. Together with molecular dynamics simulations (7), theoretical studies based on Kramers' theory, and probability density calculations (8, 9), the applied force experiments are essential for mapping the energy landscape that governs noncovalent bond strength under dynamic conditions (8). A dependence of the rupture force or bond strength on the loading rate had been predicted by theoretical calculations (8–10). Experimentally, bond strengths, sustained by weak noncovalent interactions, were recently measured at different loading rates, initially using P-selectin (11) and biotin/avidin-related systems (12). The rupture force was found to depend linearly on the natural logarithm of the loading rate revealing sharp energy barriers at fixed barrier widths (2.5 Å (120 pN $< F <$ 170 pN) for P-selectin; 30 Å (5 pN $< F <$ 10 pN), 3 Å (38 pN $< F <$ 90 pN), and 1.2 Å (90 pN $< F <$ 180 pN) for biotin/avidin; 5 Å (20 pN $< F <$ 90 pN) and 1.2 Å (90 pN $< F <$ 180 pN) for biotin/streptavidin) in the energy landscape along the dissociation pathway in the simple linear model used (11, 12). Having inspected the pathways of force-driven complex dissociations it is possible to gauge, for example, the capacity of a receptor to mediate firm or transient adhesion. As an illustration of the extent of force by multiple contacts between molecules, two sponge proteoglycan glyconectin 1 (MW 250 kDa) molecules were reported to generate 400 pN, sufficient to hold the weight of 1600 cells (13, 14). Another case for monitoring multiple contacts involving various types of molecules and forces in the nanonewton range by AFM is given for the trophoblast and uterine epithelium en route to the ensuing implantation (15).

Having proven the feasibility of introducing AFM to the evaluation of complex stability under force, several issues of biological relevance can be studied. Focusing on one type of ligand, which can serve as a docking point for more than one receptor, the stability of the complexes has so far not been monitored comparatively with this method. Four sugar receptors sharing ligand specificity but not binding site homology were selected, i.e., two plant agglutinins, a mammalian galectin, and an immunoglobulin G fraction. Although sugar receptors employ common atomic recognition modes with hydrogen bonds, van der Waals force, and stacking and hydrophobic interactions, their relative distribution in individual cases can translate into physicochemically detectable differences. They will yield distinct shapes of the energy landscape for removal of the same type of ligand from the binding pockets.

Physiologically, oligosaccharides of cellular glycoconjugates excel as information-bearing substances (16). In the interplay with lectins they serve to direct a variety of cellular functions including cell adhesion, intra- and intercellular glycoprotein routing, and cell growth (17–19). The frequent presentation of more than one carbohydrate recognition domain (CRD) in a protein molecule enables lectins to act as bridging/crosslinking molecules with relevance for mediating adhesion and eliciting signaling (18, 20–22). Since mechanical binding properties will determine the complex stability and function, we employed surface plasmon resonance (SPR) and AFM to scrutinize dynamic features of sugar receptor/carbohydrate ligand interactions at zero and increasing forces. Recently, SPR has proven valuable in the determination of the kinetic parameters of receptor-ligand pairs under zero force for lectin/glycoligand interactions (23, 24). While keeping the ligand side deliberately constant, we have chosen three lectins (two related plant lectins and a mammalian lectin) and a natural lactose-binding immunoglobulin G fraction to assess the binding properties. The plant lectins, *Ricinus communis* agglutinin (RCA), a potent crosslinker of erythrocytes, and *Viscum album* agglutinin (VAA), share the basic folding pattern and CRD presentation. The homodimeric galectin-1 (referred to as BHL, bovine heart lectin) with its CRDs at opposing ends of the protein bears no relationship to these plant agglutinins, as is also the case for the antibody. Topological properties of the binding sites and/or their presentation have previously been shown to translate into differential reactivities toward lactose-containing neoglycoconjugates and starburst glycodendrimers at equilibrium conditions (25, 26). Considering topological aspects of the ligand, computer-assisted molecular mechanics and dynamics simulations and NMR spectroscopy have delineated that VAA and a galectin can perform differential conformer selection (27–29). Evidently, the conformational states of crucial recognition sites for molecular binding are different, as corroborated by chemical mapping with ligand derivatives (30). Force-dependent kinetics, reflecting binding properties in a dynamic system, for example, under flow, have so far not been investigated.

To address this issue, first the zero-force kinetics were comparatively examined for the four receptor types, using monitoring of SPR (31, 32). In the next

recognition domain; EDC, 1-ethyl-3-(3-dimethylaminopropyl)carbodiimide; IgG, natural lactose-binding immunoglobulin G fraction; LacNAc, *N*-acetyllactosamine; NHS, *N*-hydroxysuccinimide; RCA, *Ricinus communis* agglutinin; VAA, *Viscum album* agglutinin; k_{off}, dissociation rate under zero force, natural off-rate; k^*, force-activated rate; SPR, surface plasmon resonance; PBS, phosphate-buffered saline.

step, rupture forces of the interactions between the four receptors and the common ligands lactose and asialofetuin (ASF) were measured at different piezo velocities. The experimental system and conditions were kept deliberately constant for this comparative analysis. The measured linear dependence of the rupture forces on the natural logarithm of the loading rate in the applied loading rate regime (11, 12) entails a sharp energy barrier at a fixed location, the barrier width, along the dissociation pathway (8). Thus, the barrier width of the binding potential and the force-mediated dissociation rate for each receptor-ligand pair can be derived using probability density calculations (8, 9). Nonetheless, it is demonstrated that the energy landscape of dissociation under force cannot be predicted based on zero-force dissociation kinetics and equilibrium thermodynamics. Tight binding and potent activity in hemagglutination for RCA is reflected in the dynamic measurements, whereas galectin-1 from bovine heart is apparently considerably less capable of sustaining ligand binding under force. The low k_{off} value at zero force from a surface presenting abundant β-galactosides points to the suitability of galectin-1 for being engaged in *cis*-interactions on the cell surface.

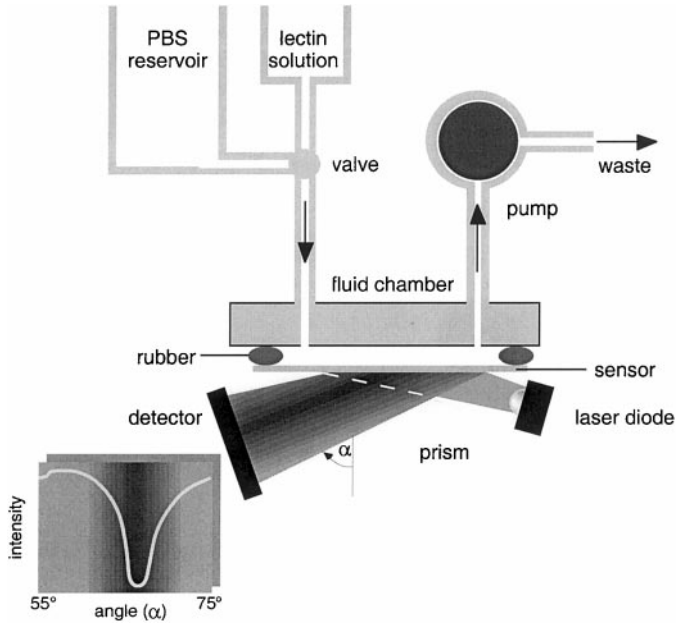

FIG. 1. Schematics of the SPR setup: The SPR sensor consists of a gold layer deposited on a glass prism. Above the sensor surface is the fluid system, which allows a constant flow through the fluid chamber of either certain molecules or PBS solution controlled by a valve. From below a divergent laser beam is reflected off the sensor surface into a line of 256 photon detectors. This detector signal is sketched at the bottom as an intensity-versus-angle plot, from which the minimum intensity of reflection is determined.

MATERIAL AND METHODS

Receptors and ligands. The ligands used in this study are lactose, bound as *p*-aminophenyl lactoside to the beads or to the cantilever, and asialofetuin (ASF). ASF as ligand was chosen because this desialylated bovine plasma protein harbors three triantennary *N*-glycan chains with either *N*-acetyllactosamine (LacNAc, 74%) or its β-1,3-isomer (9%) in the outer Man-α-1,3-arm and a biantennary chain with terminal LacNAc (17%) as a natural binding structure with proven efficiency in crosslinking assays (20, 21). The receptors used are the two plant lectins *R. communis* agglutinin (Sigma, Deisenhofen, Germany) and *V. album* agglutinin, the mammalian lectin galectin-1 (bovine heart (ga)lectin) and a natural lactose-binding immunoglobulin G fraction (IgG) from human serum.

Purification of sugar receptors. VAA, the mammalian galectin, and the immunoglobulin G fraction were purified using affinity chromatography on lactose-Sepharose 4B as the decisive step and checked for purity, as described previously (26, 33, 34).

Beads. Sepharose 4B beads exposing lactose or lectin/glycoprotein were prepared by divinyl sulfone activation and subsequent covalent attachment of the (glyco)proteins with a yield of 12 mg/ml for galectin-1 (BHL) and 10 mg/ml VAA and asialofetuin, as described previously (35). In the experimental setup lactosylated and ASF-containing beads were used to test the rupture forces for the plant lectins and the IgG exposed on the AFM cantilever. VAA and BHL beads were used to test the rupture forces for ASF- and lactose-bearing AFM cantilevers.

SPR experiments. SPR measurements were performed in a commercial instrument (Spreeta evaluation kit; Texas Instruments, Dallas, TX) connected to a flow system (see Fig. 1). The intensity of a photon beam exhibits a minimum at a certain angle when totally reflected from a thin metal layer according to the excitation of a surface plasmon resonance in the metallic surface (36). The angle of minimum reflectance is drastically influenced by slight changes in the optical density of the material at the thin metallic surface (sensor surface) in the range of the evanescent field. Hence the adsorption or desorption of molecules can cause a measurable shift of the SPR by changing the refractive index or the thickness (in the subnanometer range) of the molecular layer on that surface.

As sensor surface a 50-nm gold-coated coverslide was functionalized with 2-aminoethanethiol (Sigma, Deisenhofen, Germany) and then incubated with carboxymethylamylose, EDC, and NHS as described later for the cantilever preparation. Either ASF or *p*-aminophenyl lactoside was covalently attached to the activated amylose. The slide was placed on the sensor prism using refractive-index-matching oil ($n = 1.5135$; Zeiss, Oberkochen, Germany) and covered with a fluid chamber. In intervals of 4 s the SPR-angle ϕ of the minimum of reflectance was determined and plotted vs time. The functionalized sensor was exposed to the four different receptors dissolved in PBS at a concentration of 50 nM for at least 20 min at a permanent flow of 0.1 μl/min and a temperature of 20°C. In the same manner, the sensor was exposed to protein-free PBS in order to obtain the dissociation kinetics of the receptors from the ligand-bearing surface. The off-rate k_{off} was determined in each case by an exponential fit to the time course of the dissociation kinetics (shown in Tables II and III) using the following correlation: $\Phi \approx \Phi_0 \cdot e^{-k_{off} \cdot t}$.

AFM cantilevers. Commercially available silicon nitride cantilevers (Microlever, Park Scientific Instruments, Atos GmbH, Pfungstadt, Germany) were used for this study. The spring constants, which varied in the range of 7–15 mN/m, were calibrated using the thermal noise technique (37–39). The tips were chemically functionalized following an established protocol (40). In order to obtain an amino-group-presenting surface, the Si–OH layer of the Si_3N_4 tips was first silanized with *N′*-[3-(trimethoxysilyl)propyl]diethylenetriamine (Aldrich, Steinheim, Germany). The amino-functionalized tips were then exposed for 10 min to PBS (20 mM phosphate-buffered saline, pH 7.4) containing 50 mg/ml carboxymethylamylose (Sigma, Deisen-

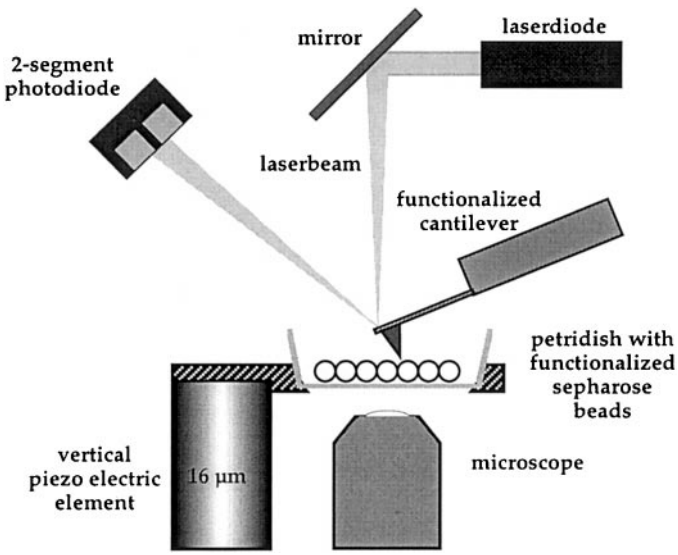

FIG. 2. The schematic diagram of the AFM setup: The protein is immobilized on the cantilever and the ligand on the Sepharose beads.

hofen, Germany), which had been activated with 10 mg/ml *N*-hydroxysuccinimide (Aldrich) and 50 mg/ml 1-ethyl-3-(3-dimethylaminopropyl)carbodiimide (Sigma). Following the reaction, the tips were rinsed in PBS to remove residual reagents and then incubated with sugar-receptor-containing solution (0.5 mg/ml solution of protein in PBS with 20 mM lactose to protect the binding pocket) or the ligand (0.5 mg/ml *p*-aminophenyl lactoside or ASF) for at least 1 h. To remove unbound glycoprotein and the lactose derivative, the tips were extensively rinsed with PBS. Force measurements were carried out in PBS solution containing 0.05–100 mM lactose as control series in the presence of a competitive inhibitor to ascertain protein-carbohydrate interactions.

AFM experiments. AFM equipment with laser-beam deflection for the force detection and a strain-gauge vertical piezo electric element for the vertical positioning, built in this laboratory, was used for the experiments (Fig. 2). To gain precise control on positioning of the probe-exposing tip on top of the Sepharose bead the AFM was mounted on an inverted microscope. In order to practically handle the vast amount of data, which can be collected, the resolution of the force curves was reduced to 8 bit for the deflection and position signals. For low piezo velocities (<3 μm/s) each data point was oversampled 15 times, for increased velocities (>3 μm/s) only 3 times. The deflection signal was low-pass filtered to reduce noise (cutoff frequency at 50 Hz for very low velocities (<0.1 μm/s) and 1 kHz for velocities beyond this limit). The bead was approached at a velocity of 1.2 μm/s in each case under controlled indentation force (typically 50 pN). For RCA and VAA between 15 and 80% of the force curves showed a rupture event after 30 ms contact time on the beads, whereas for BHL and the immunoglobulin fraction this contact time had to be increased to 60 ms to yield between 5 and 15% rupture events. For the retraction of the tip the piezo velocity was varied between 0.02 and 6 μm/s. To assess the rupture force, the loading rate and the position of the last peak, the obtained data were evaluated off-line.

RESULTS AND DISCUSSION

Noncovalent fit between complementary shapes governs molecular recognition events *in vivo*. In addition to monitoring binding strength under equilibrium conditions receptor functions can further be delineated by AFM using increasing external force to describe the energy landscape. When comparing these two data sets for receptors with identical ligand specificity, it is possible to infer to what extent the properties at zero and externally applied force are connected and a receptor is capable to maintain ligand contact under adverse conditions.

SPR Measurements

In order to determine spontaneous k_{off} values experimentally at zero force we performed SPR measurements. Initial experiments focused on RCA, yielding a value of $1.2 \pm 0.4 \times 10^{-3}$ s^{-1} when using asialofetuin as ligand. Crosslinking experiments in solution with three of the four tested sugar receptors had revealed that each of the nine glycan antennae of this glycoprotein can serve as binding partners (20, 21). Relative to a free triantennary *N*-glycan chain it can be expected that the dissociation rate from the glycoprotein will be reduced. A comparison with published data, given in Table I, verifies this assumption. The presence of lactose instead of the *N*-glycan-presenting glycoprotein only slightly affected this parameter (RCA/lactose: $1.1 \pm 0.6 \times 10^{-3}$ s^{-1}). Further measurements were directed toward addressing the question of the kinetic properties of ligand dissociation from the other sugar receptors. The off-rates under zero force measured by

TABLE I

Compilation of Off-Rates Monitored under Zero Force by SPR for Various Sugar Receptors

	RCA/ biantennary *N*-glycan[a]	RCA/ triantennary *N*-glycan[a]	RCA/ tetraantennary *N*-glycan[a]	Anticarbohydrate IgG/*O*-polysaccharide[b]	P-selectin/ PSGL-1[c,d]	L-selectin/ GlyCAM-1[e]	C-type macrophage lectin/ glycopeptides from ASF[f]	Collectin CL-43[g]
k_{off} [s^{-1}]	$3.1 \pm 0.5 \times 10^{-3}$	$1.8 \pm 0.2 \times 10^{-3}$	$1.5 \pm 0.1 \times 10^{-3}$	Slow: 1.2×10^{-2} Fast: 1.2×10^{-1}	$3.0 \pm 1.0 \times 10^{-4}$ 1.4 ± 0.1	>10	2.6×10^{-4}	$1.19–1.36 \times 10^{-2}$

[a] (63); [b](41); [c](11); [d](47); [e](64); [f](42); [g](65).

TABLE II

Kinetic Off-Rate of the Dissociation of Lactose from Four Sugar Receptors Monitored under Zero Force by SPR and Force-Mediated Parameters, Calculated by Probability Density Simulations

	RCA	VAA	BHL	IgG
		SPR		
k_{off} [s^{-1}]	$1.1 \pm 0.6 \times 10^{-3}$	$1.1 \pm 0.2 \times 10^{-3}$	$0.5 \pm 0.2 \times 10^{-3}$	$1.3 \pm 0.3 \times 10^{-3}$
		Calculation		
γ [Å]	4.1 ± 0.7	7.5 ± 1.6	10.2 ± 1.7	7.2 ± 0.9
k^* [s^{-1}]	0.8	0.09	0.09	0.9

SPR for the second plant lectin were found to be $1.1 \pm 0.2 \times 10^{-3}$ s^{-1} (VAA/lactose) and $1.3 \pm 0.5 \times 10^{-3}$ s^{-1} (VAA/ASF) (Table II and Table III). Thus, nearly equal dissociation kinetics under zero force operated for the two structurally related plant agglutinins. For the mammalian galectin and the carbohydrate-binding antibody the off-rates were found to be $0.50 \pm 0.02 \times 10^{-3}$ s^{-1} (BHL/lactose), $1.1 \pm 0.5 \times 10^{-3}$ s^{-1} (BHL/ASF), $1.3 \pm 0.3 \times 10^{-3}$ s^{-1} (IgG/lactose), and $0.55 \pm 0.03 \times 10^{-3}$ s^{-1} (IgG/ASF) (Table II and Table III).

Apparently, the different topologies and/or presentation modes of the CRDs in the lectin and the IgG will translate into their disparate behavior toward a surface, which exposed ligands with a spectrum of intermoiety distances and the triantennary *N*-glycans preferred by the IgG. For another carbohydrate-specific antibody against a bacterial lipopolysaccharide *O*-antigen the dissociation kinetics monitored by SPR (41) revealed a dependence on the dimeric structure, represented by fast (monovalent attachment) and slow off-rates for the antibody (see Table I). The slow off-rate was found to be higher compared to the off-rates for the IgG measured in this study. In comparison to the galectin, the C-type galactoside-binding lectin of macrophages, which can form dimers and trimers in solution, displayed similar dissociation kinetics under zero force (42, 43), as also given in Table I. Having explored the zero-force dissociation, we next investigated this behavior when exerting force on the complex.

AFM Measurements

Using the AFM setup, shown in Fig. 3a, the binding strength of the receptor-ligand pairs was evaluated. Each receptor and sugar ligand were covalently attached to the AFM tip and the bead, respectively. Polymer spacers between the tip material and the sensor molecule were introduced to assure sufficient distance to the surface in order to avoid restrictions of spatial accessibility (4). The processes leading to the force-piezo position curves (deflection signal vs position of the piezo), shown exemplarily in Fig. 3b, can be divided into three parts: in (i) the functionalized tip is in contact with the ligand-bearing bead for a defined period of time and the pulling of the tip starts; in part (ii) the polymer linking the receptor and the tip is stretched; in (iii) the last discontinuous jump or peak in the deflection signal corresponds to the rupture force of the receptor-ligand dissociation.

The slope of the curve ($\Delta F \cdot$ piezo velocity/Δx) calculated from the course of the curve in the section prior to the actual rupture reflects the maximum loading rate, which is referred to as loading rate in the text (Fig. 3b, ii). By applying different piezo velocities

TABLE III

Kinetic Off-Rate of the Dissociation of *N*-Glycans of ASF from Four Sugar Receptors Monitored under Zero Force by SPR and Force-Mediated Parameters, Calculated by Probability Density Simulations

	RCA	VAA	BHL	IgG
		SPR		
k_{off} [s^{-1}]	$1.2 \pm 0.4 \times 10^{-3}$	$1.3 \pm 0.5 \times 10^{-3}$	$1.1 \pm 0.5 \times 10^{-3}$	$0.5 \pm 0.5 \times 10^{-3}$
		Calculation		
γ [Å]	4.1 ± 0.7	6.0 ± 0.9	6.2 ± 0.6	4.8 ± 0.7
k^* [s^{-1}]	0.4	0.9	1.3	1.6

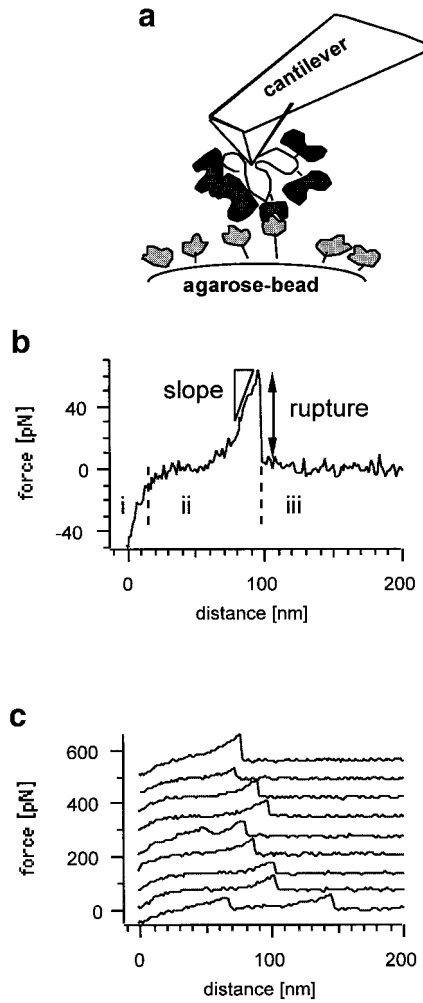

FIG. 3. (a) Experimental setup: Protein coupled via an amylose spacer to the AFM cantilever and accessible for contact with the ligands bound via a spacer bridge to a Sepharose bead. (b) Force vs piezo position curve determined in the course of gradual retraction of the AFM sensor. The slope $\Delta F/\Delta t$ is the apparent loading rate acting at the molecular bond. (c) Set of typical force-distance curves using a RCA-exposing cantilever and a Sepharose bead with covalently attached lactose moieties.

(0.02–6 μm/s) a wide range of loading rates from 10 to 20,000 pN/s was taken into account. A limit to achievable loading rates was attributable to thermal drift as well as to low force resolution at low velocities and hydrodynamic effects at high velocities. A typical set of force-distance curves recorded with the RCA/lactose pair at a piezo velocity of 1.2 μm/s is shown in Fig. 3c. Rupture events occurring when the tip is still closer than 20 nm to the surface were not considered for the data evaluation, because they were assumed to be caused by nonspecific adhesion. The dependence of the rupture forces on protein-carbohydrate interactions was confirmed for each receptor-ligand pair by reversible blocking of the binding events with lactose added to the PBS solution as competitive inhibitor. Compared to measurements in inhibitor-free PBS solution the binding probability was reduced by a factor of 10 in PBS solution containing 5 mM (for VAA) and by a factor of 80–100 for all proteins in the presence of 100 mM lactose. Having thus examined the experimental setup in the initial series, it was next possible to provide an insight into the receptors' capacity to withstand force when associated to their ligands.

In this part of the study rupture forces of the complex between the glycan and its binding protein were measured at different piezo velocities to obtain information about the dependence of the rupture force on the loading rate. Figure 4 describes the steps employed in assessing the mean rupture forces and corresponding mean loading rates at the rupture point for different piezo velocities. To obtain the statistical distribution of the rupture forces and the loading rates under the same experimental conditions force-distance curves at one given piezo velocity were recorded repeatedly (between 300 and 5000 times) with the same functionalized cantilever. Each single force-distance curve of this data set was evaluated off-line for the rupture force and the loading rate following the procedure described above. This monitoring yielded the distribution of the rupture force values and corresponding loading rates for the used piezo velocity and cantilever. The obtained data were plotted in a rupture force histogram. The dynamic properties of each receptor-ligand system were scrutinized by recording several (at least seven, as for BHL/lactose, more than seven for the other interactions) force-distance curve data sets at different piezo velocities.

In Fig. 4a the histograms of the rupture forces for the RCA/lactose pair measured at three different piezo velocities are exemplarily given (v = 4.6–1.2–0.2 μm/s). These three histograms show the effect of the variation of the piezo velocity. The maximum of the distribution was shifted from higher to lower forces with decreasing piezo velocity (70–50–35 pN). To access a basis for the calculation of the mean values of the rupture force distributions, the two-dimensional representations, shown in Fig. 4a, were extended to three-dimensional (3D) histograms (Fig. 4b) by adding the loading rate at the rupture point as abscissa. The black pixels in the 3D histogram correspond to the highest counts, whereas the white ones represent zero counts. Pixels with more than 50% of the intensity on a scale from white to gray and black were used to calculate the mean values of the rupture force and loading rate for each 3D histogram. The three calculated mean rupture forces were then plotted vs the natural logarithm of the mean loading rate including their error bars, reflecting the standard deviation, as exemplarily shown in Fig. 4c. The thickness of the error bars represents the number of rupture events considered for the calculation of

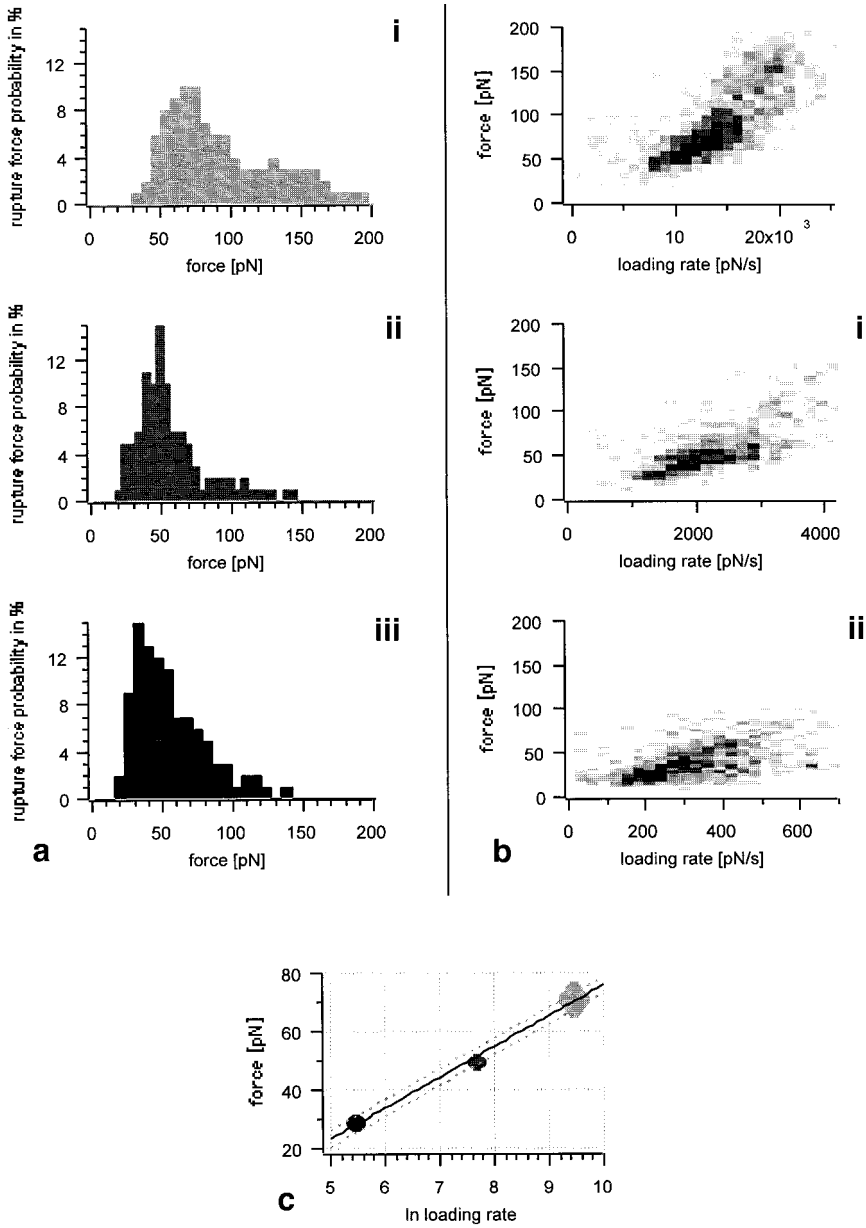

FIG. 4. (a) Histograms of RCA/lactose interaction for three different pulling velocities using the same tip in these cases. To reduce the number of multiple binding events the experiments were carried out in a solution of PBS containing 50 μM lactose. (i) 4.6 μm/s, total of 3840 force scans, 28% with rupture events. (ii) 1.2 μm/s, total of 2368 force scans, 21% with rupture events. (iii) 0.2 μm/s, total of 4480 force scans, 15% with rupture events. (b) 3D histogram of the rupture force vs loading rate distribution for the data presented in (a). The black pixels correspond to the highest counts, whereas the white ones represent zero counts. (c) Mean values for the force and loading rate plotted as crosses with the standard deviation for each pulling velocity. The linear dependence of the rupture force on the natural logarithm of the loading rate is shown by linear regression using the given sets of data.

the mean value. A linear dependence (as shown by the linear regression) of the rupture force on the natural logarithm of the loading rate was observed. This behavior had been predicted by theoretical work (8, 9), using Kramers' theory and probability density calculations. Apparently, the extent of receptor-ligand bond strengths is governed by the speed at which the ligand is pulled out of the binding pocket. With this observation further information about the binding pocket in the simple linear model used and the dissociation rate under external force can be inferred (11, 44).

Having established the experimental system to vary the loading rate and verify its operativeness, we next systematically performed measurements on each sugar receptor and the two types of ligand-bearing beads, i.e., lactose and asialofetuin. At least five different cantile-

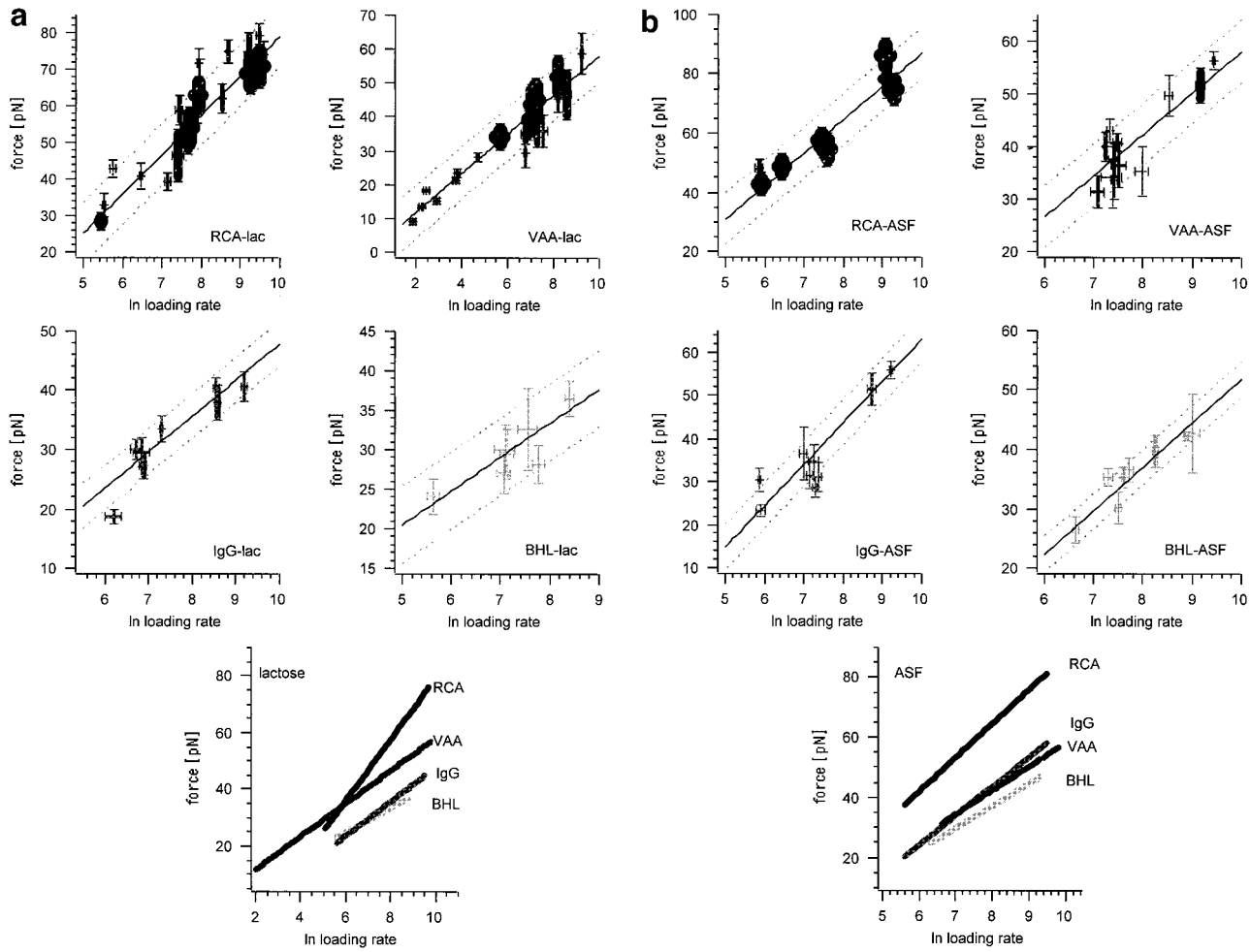

FIG. 5. Mean values of the relation between the rupture force and the natural logarithm of the loading rate for the experiments with different tips, beads, and piezo velocities for the four tested sugar receptors. The plot of each data set includes the linear regression with standard deviations for the respective receptor. For convenient comparison the regression lines for each receptor-ligand interaction are introduced into one plot at the bottom of each figure: (a) interactions with lactose as ligand, (b) interactions with the *N*-glycan chains of ASF as ligand.

vers and Sepharose beads were applied in each case. For VAA the receptor-ligand positioning on Sepharose beads and cantilevers was also switched with no visible impact on the data distribution in the respective plot, allowing a combination of these two series (Fig. 5a). The mean rupture force and the apparent mean loading rate were calculated for several piezo velocities, as described above. The mean value for one data set (one velocity, one cantilever) in force-distance curves is represented by each data point and its error bars in the graphs shown in Figs. 5a and 5b. For each of the receptor-ligand pairs the mean rupture force was found to show a linear dependence with the natural logarithm of the loading rate (see Fig. 5), represented by the linear regression of the data. However, the individual behavior was obviously different, as summarized in the bottom section of Figs. 5a and 5b.

In order to reveal similarities or disparities in the properties of the four sugar receptors in this respect, identical conditions had been defined and comparative analysis was performed (see Fig. 5a). Despite their close relationship as members of the AB toxin family of plant lectins and the equal off-rates under zero force, the two plant lectins clearly exhibited different dynamic properties. For loading rates greater than 700 pN/s (ln(700) = 6.6) the mean rupture forces of the RCA/lactose pair were higher and increasing faster with increasing loading rates than those of the VAA/lactose pair. For instance, 58 ± 9 pN for RCA and 47 ± 7 pN for VAA were measured as mean rupture forces at a loading rate of 3000 pN/s. For loading rates less than 700 pN/s the measured rupture forces for the plant lectins are comparable, as can be seen by the intersection of the linear regressions in Fig. 5a (bottom). Next,

the binding strengths of the plant lectins to the ligand lactose were compared to the property measured for the mammalian galectin BHL. Based on zero-force kinetics with lactose as ligand the off-rate of the galectin had been observed to be the lowest in this set of proteins (Table II). In the experimentally accessible loading rate regime (150–10,000 pN/s), however, the binding strengths of the plant lectins to the ligand were higher than those for the mammalian galectin (see Fig. 5a). Hence, the extended natural lifetime of the BHL/lactose bond under zero force compared to those of the plant lectins will not be sustained in the force experiments. In other words, resistance to withstand force against rupture is lower for the galectin than for RCA still sticking to its ligand. At a loading rate of 3000 pN/s the mean rupture force for the BHL/lactose pair was found to be 34 ± 6 pN compared to the 58 ± 9 pN given above for RCA.

To determine this parameter for an immunoglobulin the lactose-binding IgG fraction from human serum had been added to the panel. As can be seen in Fig. 5a, the binding strength, with 36 ± 4 pN at a loading rate of 3000 pN/s, is generally comparable in the experimental loading rate regime (150–10,000 pN/s) to the one obtained for the mammalian galectin in the interaction with lactose. Additionally, the force-distance curves probing the mammalian galectin and the IgG exhibited, even despite extended contact times of the cantilever with the bead, significantly less rupture events compared to those of the plant lectins. Thus, less rupture events were considered for the mean values shown in Figs. 5a and 5b. So far, a disaccharide has been offered as model ligand to the sugar receptors. The disparate binding strengths despite equal spontaneous off-rates (RCA and VAA) and the comparable strengths despite disparate spontaneous off-rates (BHL and IgG) intimate different mechanisms to withstand dissociation under force for the examined receptors.

To answer the question concerning the actual ranking of this parameter in the interaction of the four proteins with naturally occurring complex-type *N*-glycans we performed these experiments with ASF as ligand, complementing the corresponding SPR experiments with this glycoprotein as ligand. The results for the receptors interacting with ASF are shown in Fig. 5b. As for the lectins interacting with lactose (see Fig. 5a), higher rupture forces were found for the two plant agglutinins at the same loading rate than with the mammalian galectin in the experimentally accessible loading rate regime (400–10,000 pN/s). The mean rupture forces of RCA interacting with ASF were the highest assessed for the four receptor/ASF pairs. For instance, a rupture force of 65 ± 9 pN (RCA) was measured at a loading rate of 3000 pN/s compared to rupture forces of 43 ± 5 pN (VAA) and 37 ± 3 pN (BHL) at the same loading rate. The binding strength for the IgG/ASF pair with 45 ± 6 pN at a loading rate of 3000 pN/s was comparable to that determined for the VAA/ASF pair. This improvement in stability under force qualitatively reflects the reduced off-rates at zero force for IgG (Table II and Table III). Despite this trend, the compilations in Table II and Table III clearly caution against the possibility of attributing predictive value to zero-force data in extrapolations to the behavior under force.

To proceed from these numbers to indications for potential biological function it is instructive to consider the available data sets for force-induced dissociation, i.e., the interaction of P-selectin and a natural glycoprotein ligand (PSGL-1) and avidin/streptavidin binding to biotin (11, 12). With a natural off-rate of 3×10^{-4} s^{-1} and a rupture force of 150 pN at a loading rate of 3000 pN/s (11) P-selectin withstands dissociation under force to a higher extent than the streptavidin/biotin or avidin/biotin pairs. For these pairs at the same loading rate the rupture forces were found to be significantly lower with 85 pN (biotin/streptavidin) and 80 pN (biotin/avidin) despite their rather low natural off-rates at zero force ($k_{\text{off strep}} = 3 \times 10^{-6}$ s^{-1}; $k_{\text{off avidin}} = 4 \times 10^{-8}$ s^{-1}) (12, 45). With respect to function the differences in the dissociation kinetics under force imply an intriguing basis for P-selectin's role as a braking tool to slow down leukocytes in the bloodstream. P-selectin is involved in mediating rolling of leukocytes on endothelial cells, and the bond to its ligand is predestined to withstand force. In concert with P-selectin, L-selectin participates in mediation of rolling of leukocytes but enabling 10-fold higher velocities than P-selectin-dependent rolling (46). The spontaneous off-rate of L-selectin from a natural ligand (GlyCAM-1) with ≥ 10 s^{-1} (see Table I) is significantly higher than that of the P-selectin/PSGL-1 pair: 3×10^{-4} s^{-1} or 1×4 s^{-1} determined in two experimental settings by SPR (11, 47). The difference in the rolling velocity together with the difference in the natural off-rates suggests that there is a relation between zero-force- and force-mediated kinetics in this context. However, the inspection of the dynamic behavior of two biotin-binding proteins revealed that these complexes do certainly not resist rupture forces as well as the P-selectin (12). Therefore, extrapolations for the behavior under force from zero-force experiments can lead astray, emphasizing the necessity to complement experiments at zero force by data acquisition under force.

Evidently, the galectin, which is present on endothelial cells of blood vessels (48–51) will not readily serve as a molecular brake or glue maintaining cohesion under force, unless the density is sufficiently high to reach a level generating the required stability. These results thus have relevance for discussing the involvement of galectin-1 in the metastatic cascade and in

signaling processes (18, 52–55). As a potential adhesion molecule it can provide a specificity-enhancing grip to the extracellular matrix. Under the condition of cell migration in developmental processes or parenchymal invasion it will not impede net cell body translocation but may even guide it. Conversely, when acting as *cis*-crosslinker on the membrane zero-force kinetics will govern the stickiness. A similar reasoning applies to the plant agglutinins. To deploy the rRNA *N*-glycosidase in the cytoplasm the lectin subunit must mediate transport to the cell interior and dissociate from its ligands. The strong binding under force might explain the reduced toxicity of RCA relative to VAA (see Figs. 5a and 5b) despite their otherwise rather similar binding properties (56, 57). Besides inferring functional aspects of the sugar receptors the energy landscape of the physical process of ligand removal can be comparatively described using probability density calculations.

Probability Density Calculations for the Rupture Forces

When experimental data were analyzed by probability density calculations (8, 9) to yield physical parameters for the description of the dynamic interaction of the molecular pairs, a uniform linear dependence was observed in the plot of rupture forces vs the natural logarithm of the loading rate. This correlation translated into a sharp energy barrier in the binding potential dominating the force-mediated dissociation kinetics in the respective force regime, as recently described in the study of the energy landscapes for the biotin/avidin (streptavidin) interactions (12). In that study a concept of complex energy landscapes was for the first time introduced, which we apply to the different galactoside-binding receptors. Without any exerted force, as is the case for the SPR measurements, the transition from the bound to the free state can be described by the natural dissociation rate. According to Kramers' theory (58, 59) this natural dissociation rate depends on an oscillation frequency (λ_0), an energy barrier (ΔU) and the inverse thermal energy $\beta = 1/k_B T$:

$$\lambda = \lambda_0 \cdot e^{-\beta \cdot \Delta U} = k_{off}. \qquad [1]$$

In Fig. 6a the binding potential under zero force is shown. In this concept the ligand is seen as a point of gravity trying to cross the potential barrier in attempts with the frequency λ_0. The dissociation kinetics is dominated by the height of the energy barrier ΔU and not dependent on the shape of the potential. Under externally applied force the energy barrier is reduced by the product of the applied force (F) with the width of the potential barrier (γ). The width of the barrier is the distance between the maximum and minimum of the potential and assumed to be constant without dependence on the externally applied force in Kramers' theory. Under force the barrier is reduced by the torque $F \cdot \gamma$. Under applied force the dissociation rate λ (see Eq. [1]) is modified by the force-driven reduction of ΔU,

$$\lambda(F) = \lambda_0 \cdot e^{-\beta \cdot (\Delta U - F \cdot \gamma)} = k_{off} \cdot e^{\beta \cdot F \cdot \gamma}, \qquad [2]$$

with F referring to force and γ the width of the binding potential or barrier width. In Fig. 6b the impact of an exerted force on the potential is shown. Under force the dissociation rate $\lambda(F)$ increases exponentially, as can be seen in Eq. [2]. In the study of the force-mediated biotin/avidin dissociation kinetics (12) several data sets with different slopes of the linear dependence of the rupture force on the natural logarithm of the loading rate had been measured. This experimental setting revealed internal energy barriers ΔU_i, as exemplarily shown in Fig. 6c. The internal barriers will successively dominate the dissociation kinetics when increasing the force. The decisive barrier width will change from the outer (γ_i) to the next inner one (γ_{i+1}), when the height of the outer energy barrier ($\Delta U_i - F \cdot \gamma_i$) equals the next inner one ($\Delta U_{i+1} - F \cdot \gamma_{i+1}$), effected by the torque $F \cdot \gamma$. Additionally, the prefactor $\lambda_0 \cdot e^{-\beta \cdot \Delta U_i}$ for the exponential function of $F \cdot \gamma$ in Eq. [2] is changed to a higher value due to the lower inner energy barrier ΔU_i. Consequently, Eq. [2] is modified by considering the different energy barriers,

$$\lambda(F) = \lambda_0 \cdot e^{-\beta \cdot (\Delta U_i - F \cdot \gamma_i)} = k_i^* \cdot e^{\beta \cdot F \cdot \gamma_i}, \qquad [3]$$

with k_i^* in the following termed as the force-activated rate for the dominating energy barrier ΔU_i. At zero force and for a potential dominating the dissociation only through one energy barrier ΔU the force-activated rate (k_i^*) turns into the natural off-rate k_{off}.

In the experiments presented here only one slope for the dependence of the rupture force on the natural logarithm of the loading rate was measured for each molecular pair. To calculate the width of the sharp energy barrier and the force-activated rate, which is crucial for the determination of whether an inner energy barrier governs dissociation kinetics in the measured range, we performed probability density computations for each receptor-ligand pair. The calculations followed the concept previously presented in the studies of the strength of biomolecular bonds (8, 9). This model was adapted to our experimental system by considering the presence of an amylose spacer between the AFM tip and the receptor-ligand pair. This modified system will necessarily exhibit an inherent elastic property (see Eq. [4]) that had to be included in the ensuing calculations. The elastic property of the amylose is described by the FJC model (60) extended by the

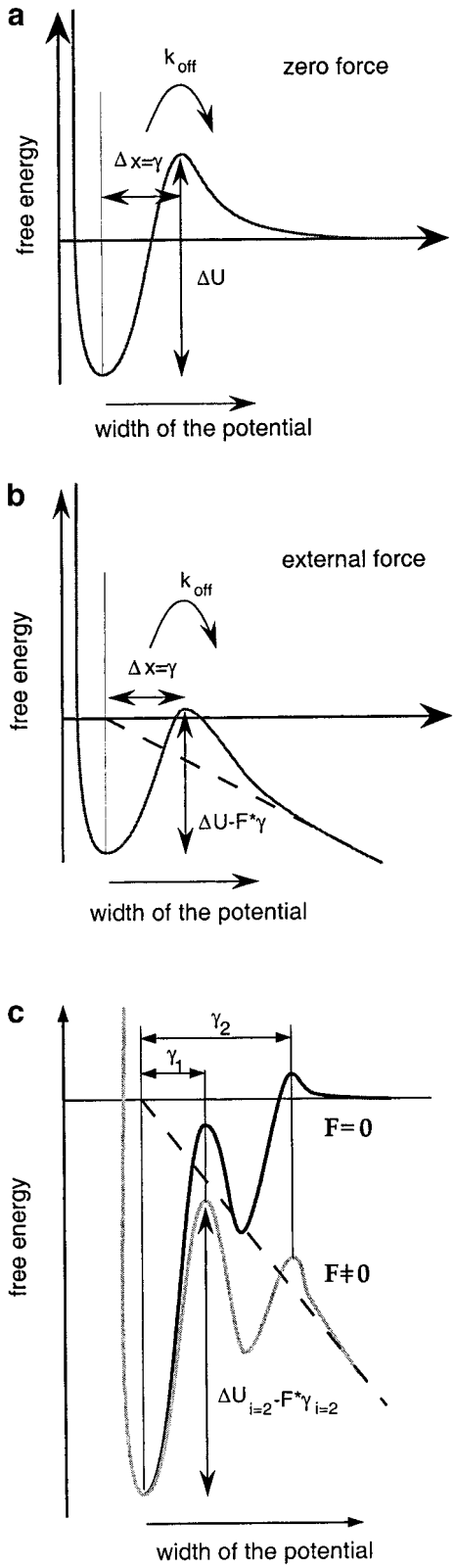

FIG. 6. Illustration of the relation between the free energy and the externally applied force: (a) potential under zero force with the energy barrier ΔU, barrier width γ, and the natural off-rate k_{off}; (b) potential under externally applied force. The energy barrier is reduced by $F \cdot \gamma$; (c) potential, schematically illustrated as given in the biotin/avidin (streptavidin) study (12). The potential is deformed under force and an internal barrier dominates the force-mediated dissociation.

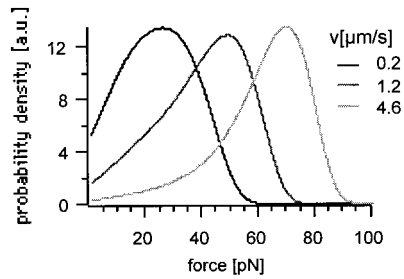

FIG. 7. Probability densities for the mean rupture forces between RCA and lactose as ligand, calculated for the three piezo velocities as used in the experiment for the data shown in Fig. 4. The two parameters determining the force-mediated dissociation kinetics, i.e., the force-activated rate (k^*) and the barrier width (γ), are given in Table II.

monomer elasticity. By considering the spring constant of the cantilever, the extension of the system under applied force is determined by

$$\langle x \rangle = N \cdot l \cdot \mathbf{L}\left(\frac{F \cdot l}{k_B \cdot T}\right) + \frac{N}{D} \cdot F + \frac{F}{k_c}. \qquad [4]$$

This expression characterizes the extension under force (F) of an amylose polymer, with N segments of the Kuhn length 1 (5.6 Å). D is the monomer elasticity (1100 pN/Å) (61), k_c the spring constant of the cantilever (1 pN/Å), and $\mathbf{L}$ the Langevin function. The amylose spacer length was chosen to be 50 nm. Equation [4], together with the piezo velocity, enables calculation of the force and loading rate applied to the ligand in the binding pocket.

As previously described (9), the force-dependent rupture probability density for a dissociation event of a receptor-ligand bond is

$$\frac{dP_{\text{diss}}}{dF}(F) = \lambda(F) \cdot \frac{1}{F} \cdot e^{-\int_0^F \lambda(f)\cdot(1/f)\cdot df}, \qquad [5]$$

with $\lambda(F)$ as the force-dependent dissociation rate (see Eq. [3]). $F(dF/dt)$ is the loading rate (see the slope in Fig. 3b) at a given force F. Hence, the probability density for the rupture is

$$\frac{dP_{\text{diss}}}{dF}(F) = k^* \cdot e^{\beta \cdot F \cdot \gamma} \cdot \frac{1}{F} \cdot e^{-k^* \cdot \int_0^F e^{\beta \cdot F \cdot \gamma} \cdot (1/f)\, df}. \qquad [6]$$

In Fig. 7 the calculated probability densities for three different piezo velocities (4.6–1.2–0.2 μm/s) for the RCA/lactose experiments, described in Fig. 4, are exemplarily presented. The force-activated rate (k^*) and the binding potential width (γ) were adjusted in the calculation to fit the experimentally obtained mean values for the maxima of the probability density distribution and the corresponding loading rates. Table II and Table III summarize the force-activated rate (k^*) and the values of the potential width (γ), obtained from the probability density calculations, for the eight receptor-sugar pairs. The potential barrier widths, reflecting the dynamical dependence of the rupture force on the loading rate, were calculated to be 4.1 $\pm$ 0.7 Å (RCA/lactose or ASF), 7.5 $\pm$ 1.6 Å (VAA/lactose), and 6.0 $\pm$ 0.9 Å (VAA/ASF) in the cases of two plant lectin-ligand binding potentials. The relative small potential barrier width for the RCA interactions reflects the resistance of RCA against bond rupture, resulting in higher rupture forces for higher loading rates (see Figs. 5a and 5b) when compared to VAA. Since the ligand side was deliberately kept constant, only properties of the protein influence the results in this experimental system. Compared to the calculated barrier widths for the mammalian galectin of 10.2 $\pm$ 1.7 Å (BHL/lactose) and of 6.2 $\pm$ 0.6 Å (BHL/ASF), a notable difference to the mistletoe lectin was observed only for the lectin/lactose interactions with a weaker dynamical dependence for BHL/lactose, whereas the VAA/ASF or BHL/ASF barrier widths were comparable. The barrier widths calculated for the immunoglobulin G fraction were 7.2 $\pm$ 0.9 Å (IgG/lactose) and 4.8 $\pm$ 0.7 Å (IgG/ASF). In aggregate, the dynamical dependence for VAA, BHL, and IgG is stronger when interacting with ASF, reflected by smaller potential barrier widths, than for lactose binding. For the RCA/ligand interaction no difference in the barrier widths was found.

The calculated force-activated rates k^* (Eq. [3], Tables II and III) for each receptor-ligand pair were consistently found to exceed the spontaneous off-rates (k_{off}) monitored by SPR. This difference signals that force-driven dissociation kinetics is dominated by an inner energy barrier, as schematically shown in Fig. 6c. Together with the barrier width this parameter describes the bond strength in the corresponding force and loading rate regime. For the plant lectins the force-activated rates were computed to be 0.8 s^{-1} (RCA/lactose), 0.4 s^{-1} (RCA/ASF), 0.09 s^{-1} (VAA/lactose), and 0.9 s^{-1} (VAA/ASF) (Table II and Table III). For mammalian galectin-1 and the immunoglobulin G fraction 0.09 s^{-1} (BHL/lactose), 1.3 s^{-1} (BHL/ASF), 0.9 s^{-1} (IgG/lactose), and 1.6 s^{-1} (IgG/ASF) were calculated (Table II and Table III). These values were confirmed by additionally performing Monte Carlo simulations, resulting in equal values for the force-activated rate but barrier widths, which were generally reduced by 0.3–0.6 Å (data not shown). The noted discrepancy between the spontaneous off-rate and the calculated rate was observed previously with the P-selectin/PSGL-1 (11) and the biotin/avidin (streptavidin) pairs (12). For the spontaneous off-rate (k_{off}), an exterior barrier width in the range of 15–40 Å is expected for all systems monitored in this study. This value can be estimated with a transition force f_{trans}, which is the lowest measurable force for an energy barrier and is in the order of $2 \cdot f_\beta$ ($f_\beta = k_B T/\gamma$), as measured for biotin-avidin interaction (12).

CONCLUSION

When probed with an AFM, complexes of different sugar receptors with a common ligand (β-galactoside) are shown to display differences in the rupture forces. It is thus documented for the first time that the stability of a sugar receptor-ligand complex involving the same disaccharide or glycan chain can vary significantly under force as a function of the protein. In this respect, the plant $(AB)_2$ toxins which are assumed to function as efficient protection against predators (62) generate a rather high level of binding strength, RCA with its potency in hemagglutination assays (56, 57) surpassing VAA. To fulfill the initial task of docking onto a surface, it is reasonable that their ligand association can withstand force. The galectin is clearly less effective in this respect. The logarithmic dependence of the mean rupture force on the loading rate enabled the calculation of parameters describing force-mediated dissociation kinetics in the context of the concept of complex energy landscapes (Fig. 6), introduced for the biotin/avidin (streptavidin) pairs recently (12). From the molecular point of view, the barrier width of the potential (γ) gives an insight into the physical energy landscape for a ligand during its dynamic interplay with the receptor's binding pocket. This parameter provides an estimation on the shape of the binding potential and the influence of increasing external force on the rupture force. Wide barrier widths account for a weak dependence, whereas tight barrier widths are correlated with a strong dependence on increasing forces. The force-activated rate (k^*) furnishes information about the deformed binding potential under externally applied force.

The calculated γ values for the receptor-lactose pairs (see Table II) intimate differences in this property for the four galactoside-binding proteins in solution. γ was found to be significantly smaller for RCA (4 Å) and greater for BHL (10 Å) in comparison to the values for VAA and IgG (both 7 Å), corroborating the measurements on the binding strength under force for each receptor/lactose pair. For example, one can readily deduce from Fig. 5a that the rupture forces of the RCA/lactose pair are the highest, while the BHL/lactose pair

is less stable at loading rates greater than 700 pN/s. When compared to the data with lactose as ligand, it can be seen that the distribution of values for the ASF-receptor pairs (Table III) is comparatively narrow. The smallest potential width for receptor/ASF interactions is still calculated for the RCA/ASF pair, and the binding in the case of RCA/ASF was found to be the strongest of the four measured receptor/ASF pairs, as shown in Fig. 5b.

When considering biologic functions, the SPR data with lactose as ligand argue in favor of a role in sustained *cis*-interactions and possibly ensuing biosignaling for galectin-1. Adhesive *trans*-interactions, which will not effectively withstand force unless a high density of receptor-ligand pairs is established, are compatible with cell migration or other transient receptor-dependent recognition processes.

When the marked differences in the behavior under force in the cases of the two related plant agglutinins are taken into account, it can be assumed that endogenous lectins from distinct or even the same family homing in on the same ligand may display a spectrum of rupture forces between cells or cells and the extracellular matrix. Exploring this assumption thoroughly can unveil new clues to explain the at-first-sight rather confusing diversification of, for example, the galectin or selectin families. Remarkably, SPR parameters at zero force harbor no reliable predictive value for properties of the tested receptors under force. AFM will thus be conducive for delineating aspects of biological functions, for example, for different galectins, warranting further studies along this route.

ACKNOWLEDGMENTS

We gratefully acknowledge valuable discussions with Stephanie Allen and Rupert Krautbauer and the financial support of the Volkswagen Foundation and the Deutsche Forschungsgemeinschaft.

REFERENCES

1. Florin, E.-L., Moy, V. T., and Gaub, H. E. (1994) *Science* **264,** 415–417.
2. Moy, V. T., Florin, E.-L., and Gaub, H. E. (1994) *Science* **266,** 257–259.
3. Dammer, U., Hegner, M., Anselmetti, D., Wagner, P., Dreier, M., Huber, W., and Güntherodt, H.-J. (1996) *Biophys. J.* **70,** 2437–2441.
4. Hinterdorfer, P., Baumgartner, W., Gruber, H. J., Schilcher, K., and Schindler, H. (1996) *Proc. Natl. Acad. Sci. USA* **93,** 3477–3481.
5. Ros, R., Schwesinger, F., Anselmetti, D., Kubon, M., Schäfer, R., Plueckthun, A., and Tiefenauer, L. (1998) *Biophysics* **95,** 7402–7405.
6. Allen, S., Davies, J., Davies, M. C., Dawkes, A. C., Roberts, C. J., Tendler, S. J., and Williams, P. M. (1999) *Biochem. J.* **341,** 173–178.
7. Grubmüller, H., Heymann, B., and Tavan, P. (1995) *Science* **271,** 997–999.
8. Evans, E., and Ritchie, K. (1997) *Biophys. J.* **72,** 1541–1555.
9. Izrailev, S., Stepaniants, S., Balsera, M., Oono, Y., and Schulten, K. (1997) *Biophys. J.* **72,** 1568–1581.
10. Heymann, B., and Grubmüller, H. (1999) *Chem. Phys. Lett.* **303,** 1–9.
11. Fritz, J., Katopodis, A. G., Kolbinger, F., and Anselmetti, D. (1998) *Proc. Natl. Acad. Sci. USA* **95,** 12283–12288.
12. Merkel, R., Nassoy, P., Leung, A., Ritchie, K., and Evans, E. (1999) *Nature* **397,** 50–53.
13. Dammer, U., Popescu, O., Wagner, P., Anselmetti, D., Güntherodt, H.-J., and Misevic, G. N. (1995) *Science* **267,** 1173–1175.
14. Misevic, G. N. (1999) *Microsc. Res. Technol.* **44,** 304–309.
15. Thie, M., Röspel, R., Dettmann, W., Benoit, M., Ludwig, M., Gaub, H. E., and Denker, H.-W. (1998) *Hum. Reprod.* **13,** 3211–3219.
16. Laine, R. A. (1997) *in* Glycosciences: Status and Perspectives (Gabius, H.-J., and Gabius, S., Eds.), pp. 1–14, Chapman and Hall, London.
17. Gabius, H.-J. (1997) *Eur. J. Biochem.* **243,** 543–576.
18. Kaltner, H., and Stierstorfer, B. (1998) *Acta Anat.* **161,** 162–179.
19. Reuter, G., and Gabius, H.-J. (1999) *Cell. Mol. Life Sci.* **55,** 368–422.
20. Gupta, D., and Brewer, C. F. (1994) *Biochemistry* **33,** 5526–5530.
21. Gupta, D., Kaltner, H., Dong, X., Gabius, H.-J., and Brewer, C. F. (1996) *Glycobiology* **6,** 843–849.
22. Villalobo, A., and Gabius, H.-J. (1998) *Acta Anat.* **161,** 110–129.
23. Shinohara, Y., Kim, F., Shimizu, M., Goto, M., Tosu, M., and Hasegawa, Y. (1994) *Eur. J. Biochem.* **223,** 189–194.
24. Okazaki, I., Hasegawa, Y., Shinohara, Y., Kamasaki, T., and Bhikhabhai, R. (1995) *J. Mol. Recogn.* **8,** 95–99.
25. Lee, R. T., Gabius, H.-J., and Lee, Y.-C. (1992) *J. Biol. Chem.* **267,** 23722–23727.
26. André, S., Cejas, P. J. O., Perez, M. A., Roy, R., and Gabius, H.-J. (1999) *Glycobiology* **9,** 1253–1261.
27. Gabius, H.-J. (1998) *Pharm. Res.* **15,** 23–30.
28. von der Lieth, C.-W., Siebert, H.-C., Kozar, T., Burchert, M., Frank, M., Gilleron, M., Kaltner, H., Kayser, G., Tajkhorshid, E., Bovin, N. V., Vliegenthart, J. F. G., and Gabius, H.-J. (1998) *Acta Anat.* **161,** 91–109.
29. Rüdiger, H., Siebert, H.-C., Solís, D., Jiménez-Barbero, J., Romero, A., von der Lieth, C.-W., Diaz-Mauriño, T., and Gabius, H.-J. (2000) *Curr. Med. Chem.* **7,** 389–416.
30. Solís, D., and Diaz-Mauriño, T. (1997) *in* Glycosciences: Status and Perspectives (Gabius, H.-J. and Gabius, S., Eds.), pp. 345–354, Chapman and Hall, London.
31. Schmitt, F.-J., Weisenhorn, A. L., Hansma, P. K., and Knoll, W. (1992) *Thin Solid Films* **210/211,** 666–669.
32. Spinke, J., Liley, M., Schmitt, F.-J., Guder, H.-J., Angermaier, L., and Knoll, W. (1993) *J. Chem. Phys.* **99,** 7012–7019.
33. Gabius, H.-J. (1990) *Anal. Biochem.* **189,** 91–94.
34. Dong, X., André, S., Hofer, B., Kayser, K., and Gabius, H.-J. (1997) *Int. J. Oncol.* **10,** 709–719.
35. Gabius, H.-J., Wosgien, B., Hendrys, M., and Bardosi, A. (1991) *Histochemistry* **95,** 269–277.
36. Kretschmann, E. (1971) *Z. Physik* **241,** 313–324.
37. Butt, H.-J., and Jaschke, M. (1995) *Nanotechnology* **6,** 1–7.
38. Florin, E. L., Rief, M., Lehmann, H., Ludwig, M., Dornmair, C., Moy, V. T., and Gaub, H. E. (1995) *Biosensors Bioelectronics* **10,** 895–901.

39. Hutter, J. L., and Bechhoefer, J. (1994) *Rev. Sci. Instrum.* **64,** 1868–1873.
40. Johnsson, B., Löfas, S., and Lindquist, G. (1991) *Anal. Biochem.* **198,** 268–277.
41. MacKenzie, C. R., Hirama, T., Deng, S. J., Bundle, D. R., Narang, S. A., and Young, N. M. (1996) *J. Biol. Chem.* **271,** 1527–1533.
42. Yamamoto, K., Ishida, C., Shinohara, Y., Hasegawa, Y., Konami, Y., Osawa, T., and Irimura, T. (1994) *Biochemistry* **33,** 8159–8166.
43. Iida, S.-I., Yamamoto, K., and Irimura, T. (1999) *J. Biol. Chem.* **274,** 10697–10705.
44. Rief, M., Fernandez, J. M., and Gaub, H. E. (1998) *Phys. Rev. Lett.* **81,** 4764–4767.
45. Green, N. M. (1975) *Adv. Protein Chem.* **29,** 85–133.
46. van der Merwe, P. A. (1999) *Curr. Biol.* **9,** R419–422.
47. Mehta, P., Cummings, R. D., and McEver, R. P. (1998) *J. Biol. Chem.* **273,** 32506–32513.
48. Gabius, H.-J., Brehler, R., Schauer, A., and Cramer, F. (1986) *Virch. Arch. B* **52,** 107–115.
49. Debbage, P. L., Gabius, H.-J., Bise, K., and Marguth, F. (1988) *Eur. J. Cell Biol.* **46,** 425–434.
50. Lotan, R., Belloni, P. N., Tressler, R. J., Lotan, D., Xu, X.-C., and Nicolson, G. L. (1994) *Glycoconj. J.* **11,** 462–468.
51. Baum, L. G., Seilhamer, J. J., Pang, M., Levine, W. B., Beynon, D., and Berliner, J. A. (1995) *Glycoconj. J.* **12,** 63–68.
52. Gabius, H.-J. (1997) *Cancer Invest.* **15,** 454–464.
53. Hirabayashi, J. (1997) *Trends Glycosci. Glycotechnol.* **9,** 1–180.
54. Ohannesian, D. W., and Lotan, R. (1997) *in* Glycosciences: Status and Perspectives (Gabius, H.-J., and Gabius, S., Eds.), pp. 459–469, Chapman and Hall, London.
55. André, S., Kojima, S., Yamazaki, N., Fink, C., Kaltner, H., Kayser, K., and Gabius, H.-J. (1999) *J. Cancer Res. Clin. Oncol.* **125,** 461–474.
56. Saltvedt, E. (1976) *Biochim. Biophys. Acta* **451,** 536–548.
57. O'Hare, M., Roberts, L. M., and Lord, J. M. (1992) *FEBS Lett.* **299,** 209–212.
58. Bell, G. I. (1978) *Science* **200,** 618–627.
59. Hänggi, P., Talkner, P., and Borkovec, M. (1990) *Rev. Mod. Phys.* **62,** 251–341.
60. Smith, S. B., Cui, Y., and Bustamante, C. (1996) *Science* **271,** 795–798.
61. Marszalek, P. E., Oberhauser, A. F., Pang, Y. P., and Fernandez, J. M. (1998) *Nature* **396,** 661–664.
62. Rüdiger, H. (1997) *in* Glycosciences: Status and Perspectives (Gabius, H.-J., and Gabius, S., Eds.), pp. 415–438, Chapman and Hall, London.
63. Shinohara, Y., Sota, H., Kim, F., Shimizu, M., Gotoh, M., Tosu, M., and Hasegawa, Y. (1995) *J. Biochem.* **117,** 1076–1082.
64. Nicholson, M. W., Barclay, A. N., Singer, M. S., Rosen, S. D., and van der Merwe, P. A. (1998) *J. Biol. Chem.* **273,** 763–770.
65. Holmskov, U., Fischer, P. B., Rothmann, A., and Hojrup, P. (1996) *FEBS Lett.* **343,** 314–316.